Research on denoising of joint detection signal of water quality with multi-parameter based on IEEMD*

LI Wen, LI Dejian, MA Yongyue, TIAN Wang, WEN Xin, and LI Jie**

Institute of Mechanical and Electrical Engineering, North China University of Technology, Beijing 100144, China

(Received 16 May 2023; Revised 9 August 2023)

An improved ensemble empirical mode decomposition (IEEMD) is suggested to process water quality spectral signals in order to address the issue that noise interference makes it difficult to extract and evaluate water quality spectral signals. This algorithm effectively solves the problems of modal mixing, poor reconstruction accuracy in the empirical mode decomposition (EMD), and a large amount of calculation in the ensemble empirical mode decomposition (EEMD). Based on EEMD, IEEMD firstly preprocesses the original water quality spectral signals, then performs Savitzky-Golay (S-G) smoothing on the decomposed effective intrinsic mode function (IMF) components, and finally reconstructs them to obtain the denoised signals. Water sample data at different concentrations can be accurately analyzed based on the noise-reduced spectral signals. In this paper, three water quality parameters are used as research objects: benzene (C_6H_6), benzo(b)fluoranthene ($C_{20}H_{12}$), and chemical oxygen demand (COD). The original water quality multi-parameter (C_6H_6, $C_{20}H_{12}$, COD) spectral signals were subjected to denoising based on the IEEMD and the water quality multi-parameter joint detection technology. The signal-to-noise ratio (*SNR*) and the correlation coefficient (R^2) of the fitted curves obtained from the processing of the IEEMD were compared and analyzed with those obtained from the processing of the EMD and the EEMD. The experimental results show that the *SNR* of the spectral signals and the R^2 of the fitting curve in three water quality parameters have been significantly improved. Therefore, the IEEMD effectively improves the phenomenon of modal mixing, reduces the amount of calculation, improves the reconstruction accuracy, and provides an important guarantee for the effective extraction of multi-parameter spectral signals of water quality.

Document code: A **Article ID:** 1673-1905(2024)02-0107-9

DOI https://doi.org/10.1007/s11801-024-3089-2

Spectroscopic analysis has been widely used in the military, science and technology, industry, medicine, and other fields[1,2]. In the field of water quality detection, the spectral analysis method has the advantages of low cost, no reagents, and multi-parameter detection. During the stage when the spectrometer converts the optical signal into an electrical signal, the humidity, temperature, and stray light in the external environment can also affect the detection process[3]. Therefore, when the spectrometer collects signal data, a large number of irrelevant interference signals will, to a certain extent, affect the acquisition of the true signal, which reduces the accuracy and stability of water quality detection[4,5].

Since most of the spectral signals in water quality detection are nonlinear, non-smooth random signals, traditional methods such as the Fourier transform cannot meet the demand for the analysis of such signals[6]. Empirical mode decomposition (EMD) is a novel algorithm proposed by HUANG et al[7] in 1998 to deal with nonlinear and nonstationary signals adaptively. The algorithm first performs an EMD of the signal to obtain multiple intrinsic mode function (IMF) components. The advantage of this algorithm is that the mode functions can better reflect the local characteristics of the signal in the time and frequency domains, so it is very suitable for processing and studying spectral signals that are neither smooth nor linear. However, this algorithm also has the shortcoming that when there is a jump change in the time scale of the signal, the IMF components obtained from the decomposition contain different time scale feature components, namely, modal mixing. To suppress the problem of modal mixing, WU et al[8] proposed the ensemble empirical mode decomposition (EEMD), the algorithm preprocesses the signal before performing EMD, so it can inherit all the advantages of EMD and effectively suppress the problem of modal mixing that is generated by EMD, but the EEMD integrates more times, which leads to a large amount of computation, and increases the error after signal processing because it cannot eliminate the added auxiliary white noise. To address the issue that the

* This work has been supported by the National Natural Science Foundation of China (No.51205005), and the Beijing Science and Technology Innovation Service Ability Building (No.PXM2017-014212-000013).

** E-mail: ldj5022729@126.com

EEMD cannot be reconstructed accurately, an improved ensemble empirical mode decomposition (IEEMD) is proposed, this algorithm achieves near-perfect signal reconstruction, and improves the phenomenon of modal mixing, which is a significant upgrade to the EEMD.

This paper focuses on the detection of C_6H_6, $C_{20}H_{12}$, and chemical oxygen demand (COD) concentrations in water samples, and the spectral signals of multi-parameter (C_6H_6, $C_{20}H_{12}$, COD) of water quality are analyzed by the IEEMD combined with multi-parameter joint detection technology of water quality. The effectiveness and practicability of the IEEMD were verified by analyzing and comparing the signal-to-noise ratio (*SNR*) and correlation coefficient (R^2) of the fitting curve obtained by three algorithms after processing spectral signals.

The EMD decomposes the signal into a number of IMFs based on the temporal characteristics of the signal. Firstly, determine all local maximum and minimum points of the signal; secondly, use the cubic spline interpolation function to construct the upper and lower envelopes and calculate the mean value curve; finally, find the difference between the signal and the mean value curve, determine whether it meets the definition of IMF, and according to the filtering stopping conditions, repeatedly judge and filter until the last remaining part of the signal is a monotonic signal, then the decomposition is finished[9].

In the process of processing signals by EMD, the presence of interfering signals leads to an abnormal distribution of local extremepoints, which will produce distortion and modal mixing, namely, an IMF component contains a variety of signals with different scales or frequencies. Modal mixing not only leads to errors in the time-frequency distribution of the signal, but also causes the IMF to lose its physical meaning, which seriously affects the accuracy of the signal processed by the EMD[10].

The EEMD is proposed to address the problem of modal mixing in EMD. The principle is to randomly add auxiliary white noise to the original signal and perform the EMD according to the characteristic that the mean value of auxiliary white noise is zero and the results of the decomposition are averaged many times, which can suppress the influence of auxiliary white noise on the decomposition results[11].

The EEMD has its own problems of high integration times and inability to eliminate the added auxiliary noise, resulting in large computations and poor reconstruction accuracy, the IEEMD is proposed to make up for the shortcomings of the above algorithm.

Firstly, the original signal is preprocessed before being processed by the IEEMD, so as to smooth the peak noise. Assume that the original signal is $y(t+1) > y(t)$, and the difference is $d = y(t+1) - y(t)$. The calculation process for the difference between the front and rear points can be calculated as follows[12]

$$y(t+1) = y(t+1) - d/2, \tag{1}$$

$$y(t) = y(t) + d/2. \tag{2}$$

The distance between high-frequency noise and low-frequency noise is reduced, the peak noise is smoothed, and the subsequent effect of modal mixing can be effectively reduced through differential pretreatment of water quality spectral signals.

The auxiliary white noise signals $m_n(t)$ and $-m_n(t)$ with zero mean are added to the original signal $y(t)$, respectively, namely:

$$y_n^+(t) = y(t) + a_n m_n(t), \tag{3}$$

$$y_n^-(t) = y(t) - a_n m_n(t), \tag{4}$$

where $m_n(t)$ represents the added auxiliary white noise signal, a_n represents the amplitude of the added noise signal, and Ne represents the logarithm of the added auxiliary white noise.

The EMD is for $y_n^+(t)$ and $y_n^-(t)$, respectively, to obtain the first order IMF component sequence $\{IMF_{n1}^+(t)\}$ and $\{IMF_{n1}^-(t)\}$ $(n = 1, 2, \cdots, Ne)$, and integrate and average the above components:

$$IMF_1(t) = \frac{1}{2Ne}\sum_{n=1}^{Ne}[IMF_{n1}^+(t) + IMF_{n1}^-(t)]. \tag{5}$$

If $IMF_1(t)$ is an abnormal signal, continue to perform the above steps until the IMF component $IMF_n(t)$ is not an abnormal signal[13]. Separate the decomposed first $(n-1)$ components from the original signal, namely:

$$r(t) = y(t) - \sum_{i=1}^{n-1} IMF_i(t). \tag{6}$$

Then the residual signal $r(t)$ is decomposed by EMD, and all IMF components are arranged from high frequency to low frequency.

Among them, the noise signal mainly exists in the high-frequency signal, while the effective signal is mainly distributed in the low-frequency IMF component, so the signal restructuring needs to determine the critical point of the IMF component of the noise signal and the effective signal. In the process of processing the signal, there is a certain correlation between each IMF component and the original signal, and the location where the correlation coefficient of the IMF component first changes abruptly can be used as the critical point to distinguish between the noisy signal and the effective signal[14].

Secondly, Savitzky-Golay (S-G) smoothing is used to further smooth the components after IEEMD processing, which can maximize the retention of these distributional properties of relative extrema and widths while removing the noise of the water quality spectral signals, as follows[15].

Assuming that the decomposition of a frequency band component from $-F$ to F has a total of $2F+1$ signal points, the kth order polynomial can be fitted to it.

$$p(t) = \sum_{i=0}^{n} a_i t^i. \tag{7}$$

Its fitting error is

$$\varepsilon = \sum_{i=-F}^{F} \left(p(t) - IMF(t) \right)^2 = \sum_{i=-F}^{F} \left(\sum_{i=0}^{n} a_i t^i - IMF(t) \right)^2 . \quad (8)$$

To obtain a_i, introduce the auxiliary matrix $\boldsymbol{C}$.

$$\boldsymbol{C} = \{c_{t,j}\}, c_{t,j} = t^j, -F \leqslant t \leqslant F, 0 \leqslant j \leqslant n. \quad (9)$$

Set another auxiliary matrix $\boldsymbol{B}$ such that

$$\boldsymbol{B} = \boldsymbol{C}^{\mathrm{T}} \boldsymbol{C} = \{b_{j,i}\}, \quad (10)$$

$$b_{j,i} = \sum_{i=-F}^{F} 2t^j c_{j,t} c_{t,i} = \sum_{i=-F}^{F} t^{j+i} = b_{i,j}. \quad (11)$$

Definition:

$$\boldsymbol{x} = \begin{pmatrix} IMF(-F) \\ \cdots \\ IMF(F) \end{pmatrix}, \quad \boldsymbol{a} = \begin{pmatrix} a_0 \\ \cdots \\ a_k \end{pmatrix}. \quad (12)$$

According to Eq.(8), it can be determined that

$$\boldsymbol{B}\boldsymbol{a} = \boldsymbol{C}^{\mathrm{T}} \boldsymbol{C} \boldsymbol{a} = \boldsymbol{C}^{\mathrm{T}} \boldsymbol{x}, \quad (13)$$

$$\boldsymbol{a} = (\boldsymbol{C}^{\mathrm{T}} \boldsymbol{C})^{-1} \boldsymbol{C}^{\mathrm{T}} \boldsymbol{x} = \boldsymbol{H}\boldsymbol{x}. \quad (14)$$

The polynomial coefficient matrix $\boldsymbol{a}$ is derived and then substituted into Eq.(7) to obtain the IMF component after S-G smoothing.

IMF components reconstruction is to screen out the IMF components with high correlation coefficients and superimpose them with residual components so as to get the denoised water quality spectral signal[16].

$$Y(t) = \sum_{i=k}^{n} IMF_i + r(t), \quad (15)$$

where $Y(t)$ is the reconstructed signal, and k is the order of the first abrupt change in the IMF correlation coefficient.

The experimental instruments include TM01-1P, normally closed solenoid valve, base pump, high-precision vertical injection pump, liquid inlet error ≤1%, AVANTES, high-resolution spectrometer, response range from 180 nm to 1 200 nm, deuterium-halogen tungsten light, emission spectra from 190 nm to 2 500 nm, mercury light, the emission wavelength of 254 nm, and multi-channel selector valves.

The experimental reagents are as follows. Experimental water is the deionized water in the "GB 11446-1-2013 National Standard for Deionized Water", preparation of standard stock solution for $KMnO_4$ in accordance with "GB11892-89", with concentration (1/5 $KMnO_4$) about 0.1 mol·L^{-1}, concentration (1/2 $Na_2C_2O_4$) about 0.01 mol·L^{-1}, (1+3) H_2SO_4, prepare the standard solution for C_6H_6 and $C_{20}H_{12}$ according to "GBW (E) 080913", and standard solution for COD.

The water sample concentration setting is as follows. Configure the standard solution for C_6H_6 with concentrations of 0.001 mg·L^{-1}, 0.01 mg·L^{-1}, 0.1 mg·L^{-1}, 1 mg·L^{-1}, 10 mg·L^{-1}. Configure the standard solution for $C_{20}H_{12}$ with concentrations of 0.000 4 mg·L^{-1}, 0.001 mg·L^{-1}, 0.004 mg·L^{-1}, 0.01 mg·L^{-1}, and 0.1 mg·L^{-1}. Configure the standard solution for COD with concentrations of 1 mg·L^{-1}, 2 mg·L^{-1}, 4 mg·L^{-1}, 6 mg·L^{-1}, and 8 mg·L^{-1}. Five different concentrations of water samples were prepared for each water quality parameter, and there were six sets of parallel experiments for each concentration of water samples.

The fluorescence intensity of the same substance excited by a light beam with the same wavelength is different according to the concentration of the substance, so the concentration of the substance can be determined by this property. According to the method of fluorescence analysis, the solutions with low relative concentrations can be detected, and the relationship between the variables is as follows[17]

$$I_{\mathrm{f}} = 2.303 \phi I_0 \varepsilon b c, \quad (16)$$

where I_{f} is fluorescence intensity, ϕ is the fluorescence quantum yield, I_0 is the incident light intensity, ε is the molar absorption coefficient, b is the thickness of the water quality detecting room, and c is the fluorescent substance concentration in water samples.

According to Beer-Lamber law, the absorbance value of each standard water sample was obtained and combined with Eq.(17) to obtain the concentration value of the solution to be measured[18].

$$A = \lg\left(\frac{I_0}{I}\right) = \varepsilon c b = Kc = -\lg\left(\frac{S-D}{R-D}\right) \times 100\%, \quad (17)$$

where A is the absorbance of the water sample, I_0 is the incident light, I is the transmitted light intensity, ε is the molar absorption coefficient, c is the concentration, b is the optical path, S is the photoelectric signal after reagent digestion, R is the photoelectric signal when the light source is on, and D is the photoelectric signal when the light source is off.

This system used fluorescence spectroscopy and UV-visible spectroscopy together, the standard solutions of C_6H_6, $C_{20}H_{12}$, and COD were measured separately, and the regression functions of each detected parameter were constructed by using the least squares method to obtain the wavelength-intensity standard curve and the wavelength-absorbance standard curve.

Firstly, after the action of the high-precision vertical syringe pump and multi-channel selector valve, the COD and reagents were put into the digestion chamber sequentially and energized for 15—20 min, and the digestion reaction was carried out under high-temperature conditions. At this time, the multi-channel selector valve was switched to the C_6H_6 and $C_{20}H_{12}$ reagent lines in turn, and the two solutions were injected sequentially into the detection chamber and scanned for determination directly by the spectrometer after being stabilized. The wavelength-intensity curves for C_6H_6 and $C_{20}H_{12}$ are shown in Fig.1(a) and (b). After the COD in the digestion chamber was digested, it was shunted to the detection chamber for scanning and determining by the spectrometer. The wavelength-absorbance curves for COD

are shown in Fig.1(c).

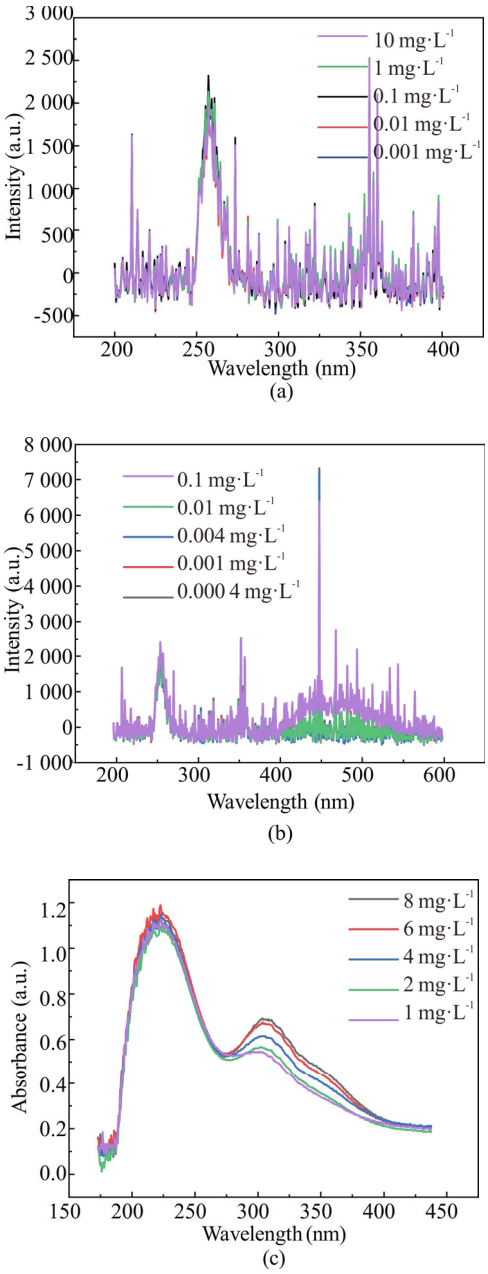

Fig.1 Original spectral signals for (a) C_6H_6, (b) $C_{20}H_{12}$, and (c) COD

The experiment required to design and build is a sequential injection spectrum analysis platform based on continuous spectrometry, as shown in Fig.2. The system is divided into four main modules: the sequential injection module, the high-temperature confinement ablation module, the light source detection module, and the terminal control display module. The reservoir loop and the reagent flow path in the sequential injection module are made of polytetrafluoroethylene (PTFE). The high-temperature confinement ablation module adopted the method of resistance wire winding ablation tube for high-temperature confinement heating. The light source detection module consists of a mercury light, a deuterium-halogen tungsten light, and a high-resolution spectrometer. The terminal control display module adopted a 32-bit high-precision MCU in the STM32F103 series as the main control chip, which communicates with the syringe pump and valve island via RS-232 and directly displays the system status and sequence for reagent and water sample feeding in real time. Within the limited space of the whole system, the four modules were reasonably distributed to achieve miniaturization and portability.

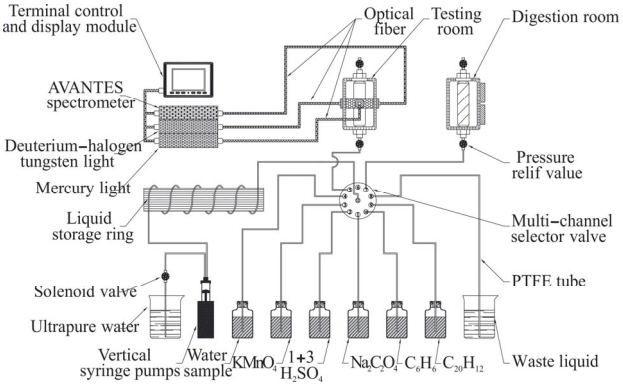

Fig.2 Schematic diagram of experimental platform

The signal obtained by scanning water samples with the spectrometer belongs to "non-linear and non-stationary" signals, and the collected spectral signals were processed by EMD, EEMD, and IEEMD, respectively. Select the C_6H_6 spectral signal with a concentration of 0.1 mg·L^{-1}, as shown in Fig.3. In this experiment, the spectral data with a wavelength of 200—400 nm was extracted and analyzed in the above way. The decomposition results of EMD, EEMD, and IEEMD are shown in Fig.4.

From the analysis of Fig.4, it can be seen that the EMD shows obvious modal mixing due to the interference of noise signals. The EEMD better overcomes modal mixing by adding the white noise to decompose the signal and going through several integrated averagings, but the decomposition process involves several iterative operations, resulting in an increase in the amount of computation, and the result of its decomposition has eight IMF components. Compared with the EEMD, the IEEMD decomposition not only suppresses modal mixing, but also reduces the number of calculations in the decomposition process, and the result of its decomposition has six IMF components, and the computational amount is significantly reduced.

The correlation coefficients μ_i, μ_j, μ_k (i, j=1, 2,...,8) between IMF components decomposed by EMD, EEMD, and IEEMD and the original spectral signals are obtained respectively, as shown in Tab.1.

Through the above three algorithms to process and analyze the spectral signals, the IEEMD can not only effectively reduce the modal mixing and computation when analyzing the spectral signals, but also ensure that

the decomposition of the component signals is basically in a stable state. According to the data in Tab.1, it can be seen that the correlation coefficients of the IMF components obtained from the original spectral signal processed by EMD, the correlation coefficient of the IMF3 component suddenly changed, so the components with low correlation coefficients before the sudden change, namely the IMF1 and the IMF2, were removed, and the remaining effective IMF components were retained. In the same way, among the IMF components obtained from the original spectral signals processed by EEMD and IEEMD, the correlation coefficients of the IMF5 in EEMD and the IMF4 in IEEMD components are abrupt. The effective IMF components processed by EMD and EEMD are reconstructed to obtain the spectral signal of C_6H_6 at a concentration of 0.1 mg·L^{-1} after denoising. The effective IMF components after IEEMD processing was subjected to S-G smoothing and then recombined to obtain the spectral signal of C_6H_6 with the same concentration after denoising. The wavelength-light intensity curves of the 0.1 mg·L^{-1} C_6H_6 spectral signal before and after denoising by EMD, EEMD and IEEMD, respectively are shown in Fig.5.

After the spectral signal is processed by the EMD, the IMF components have the problem of modal mixing, so the reconstructed signal contains a small number of interference components, which will affect the calibration of the working curve and the accuracy of water quality detection. The C_6H_6 spectral signal is processed by the EEMD, which is more computationally intensive, although it effectively suppresses the modal aliasing phenomenon. Moreover, if the amplitude and iteration times of adding auxiliary white noise are not appropriate, there will be more false components in the decomposition, which may affect the effect of denoising. As can be seen from Fig.5(b), the C_6H_6 spectral signal still contains a small number of interference components after noise reduction by the EEMD, and the interference is obvious in the emission band from 350 nm to 360 nm. Compared with the EMD and the EEMD for denoising, the IEEMD performs denoising on the C_6H_6 spectral signals, and the processed signals are relatively smooth and have relatively fewer interference components.

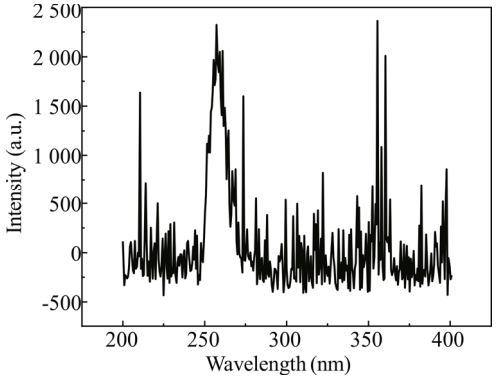

Fig.3 Original spectral signal of C_6H_6 with a concentration of 0.1 mg·L^{-1}

Tab.1 The correlation coefficients between the IMF components and the original spectral signal by three algorithms

IMF component	μ_i (EMD)	μ_j (EEMD)	μ_k (IEEMD)
IMF1	0.436 4	0.033 4	0.041 5
IMF2	0.263 6	0.044 1	0.036 8
IMF3	0.503 3	0.025 2	0.048 1
IMF4	0.481 2	0.056 3	0.397 9
IMF5	0.460 2	0.366 9	0.561 9
IMF6	0.281 8	0.404 0	0.441 6
IMF7	—	0.556 8	—
IMF8	—	0.398 4	—

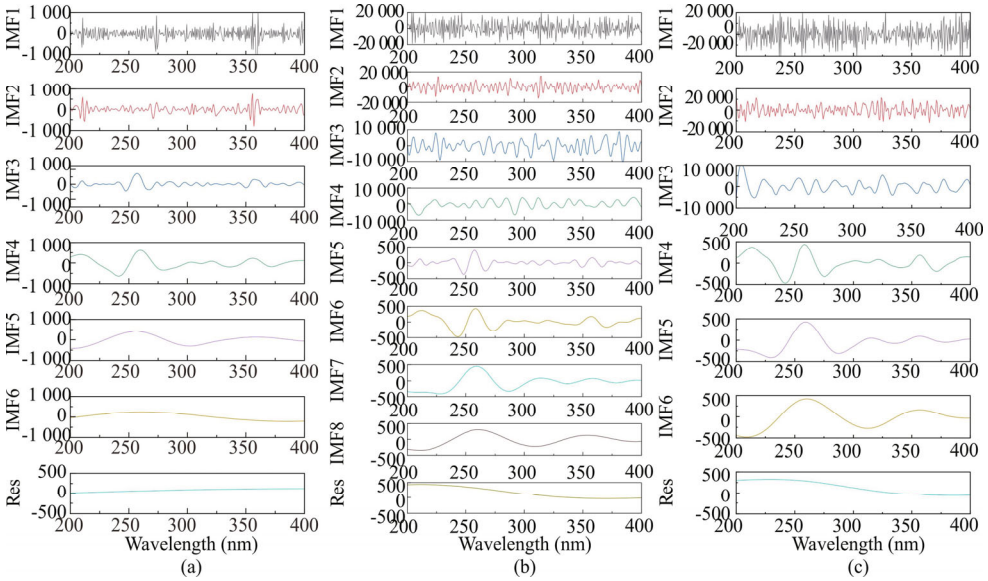

Fig.4 Spectral signals decomposition by (a) EMD, (b) EEMD, and (c) IEEMD

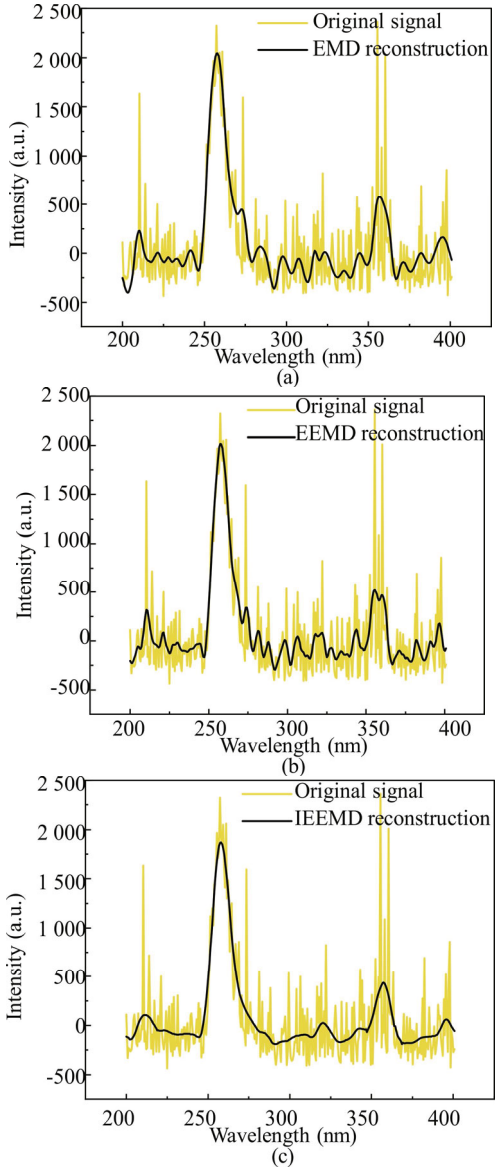

Fig.5 Denoising of spectral signals of C_6H_6 with a concentration of 0.1 mg·L^{-1} by (a) EMD, (b) EEMD, and (c) IEEMD

Similarly, the denoising of the spectral signals of C_6H_6, $C_{20}H_{12}$ and COD at different concentrations was carried out by the above three algorithms, respectively, and the results are shown in Fig.6. The excitation peak wavelength of C_6H_6 and $C_{20}H_{12}$ is about 254 nm, while the emission peak wavelength of C_6H_6 is about 357 nm, the emission peak wavelength of $C_{20}H_{12}$ is about 396 nm, and the absorption peak wavelength of COD is about 304 nm.

To verify the superiority of the IEEMD, the *SNR* of the spectral signals of C_6H_6, $C_{20}H_{12}$ and COD at different concentrations was verified by comparing the three algorithms, and the specific index was calculated as follows[19]

$$SNR = 10\log\frac{\sum_{i=1}^{n} Y(t_i)^2}{\sum_{i=1}^{n}\left[y(t_i)-Y(t_i)\right]^2}. \tag{18}$$

The *SNR* statistics of the three algorithms for processing the spectral signals of C_6H_6, $C_{20}H_{12}$ and COD at different concentrations are shown in Tab.2, which shows that the IEEMD has significantly improved the *SNR* after denoising for three parameters compared to the EMD and the EEMD.

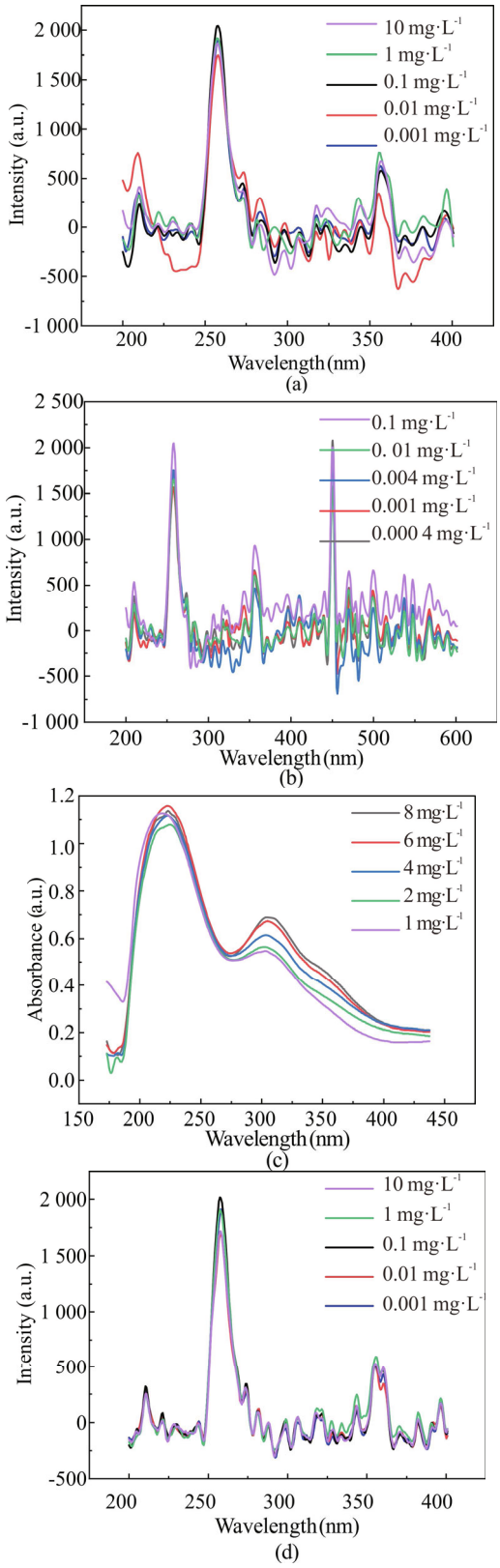

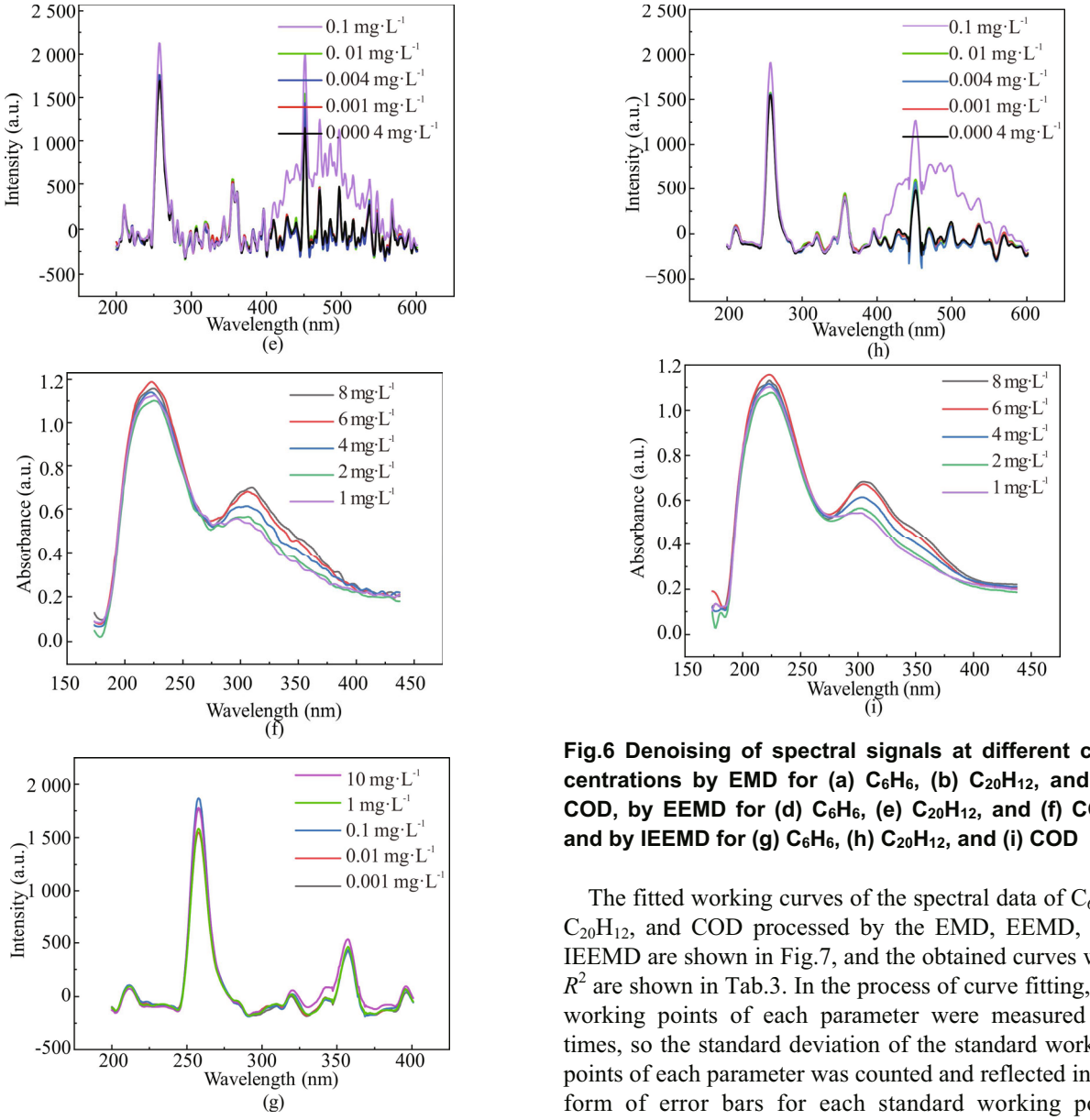

Fig.6 Denoising of spectral signals at different concentrations by EMD for (a) C_6H_6, (b) $C_{20}H_{12}$, and (c) COD, by EEMD for (d) C_6H_6, (e) $C_{20}H_{12}$, and (f) COD, and by IEEMD for (g) C_6H_6, (h) $C_{20}H_{12}$, and (i) COD

The fitted working curves of the spectral data of C_6H_6, $C_{20}H_{12}$, and COD processed by the EMD, EEMD, and IEEMD are shown in Fig.7, and the obtained curves with R^2 are shown in Tab.3. In the process of curve fitting, the working points of each parameter were measured six times, so the standard deviation of the standard working points of each parameter was counted and reflected in the form of error bars for each standard working point

Tab.2 Comparison of the denoising effect of the spectral signals of C_6H_6, $C_{20}H_{12}$ and COD at different concentrations by three algorithms (*SNR*)

C_6H_6 ($mg·L^{-1}$)	*SNR* (EMD) (dB)	*SNR* (EEMD) (dB)	*SNR* (IEEMD) (dB)	$C_{20}H_{12}$ ($mg·L^{-1}$)	*SNR* (EMD) (dB)	*SNR* (EEMD) (dB)	*SNR* (IEEMD) (dB)	COD ($mg·L^{-1}$)	*SNR* (EMD) (dB)	*SNR* (EEMD) (dB)	*SNR* (IEEMD) (dB)
0.001	2.398 8	2.992 4	3.087 8	0.000 4	1.091 2	2.486 6	2.522 0	1	32.682 7	31.520 4	35.546 6
0.01	1.405 1	1.755 9	2.264 7	0.001	1.171 7	2.094 2	2.774 6	2	31.451 6	31.108 1	34.648 5
0.1	2.742 3	2.987 7	3.589 4	0.004	1.942 3	2.337 8	3.040 5	4	34.719 2	33.797 4	37.780 5
1	2.493 7	2.752 3	3.097 4	0.1	1.970 6	1.910 2	2.429 7	6	33.098 9	31.589 9	35.779 8
10	1.226 3	1.605 6	2.838 8	1	1.160 7	1.022 7	1.359 1	8	20.735 9	19.074 9	22.722 3

in Fig.7. According to the results in Tab.3, compared with the EMD and the EEMD for the spectral signal of three parameters, the fitted curve obtained by the IEEMD is less deviated, so the standard working curve drawn by the IEEMD is highly reliable and stable.

An algorithm for IEEDM is suggested to process water quality spectral signals in order to address the issue that noise interference makes it difficult to extract and evaluate water quality spectral signals. The issues of modal mixing, low reconstruction accuracy in the EMD, and a significant amount of computing in the EEMD are all successfully resolved by the IEEMD. Three water

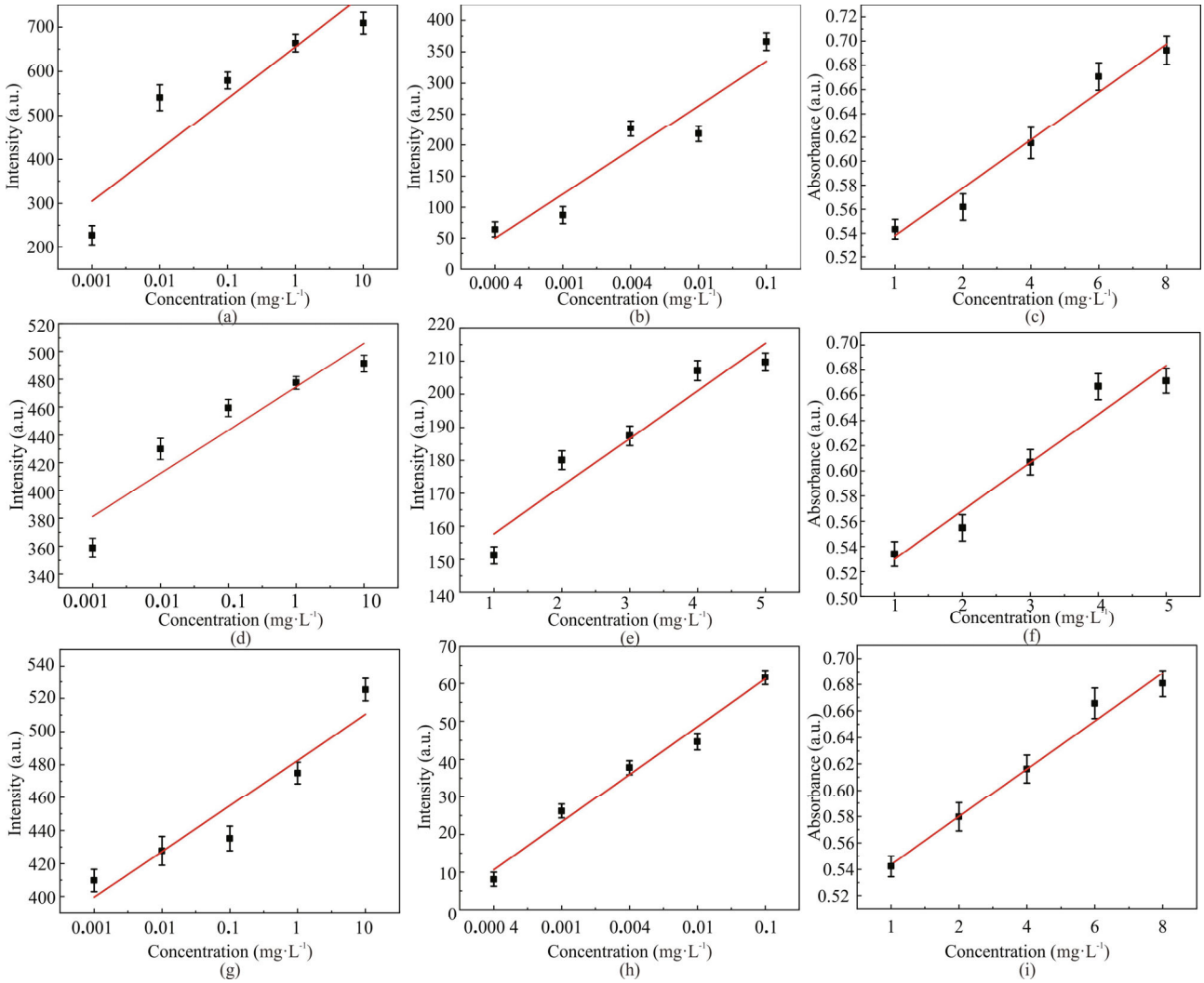

Fig.7 EMD processed results for (a) C_6H_6, (b) $C_{20}H_{12}$, and (c) COD; EEMD processed results for (d) C_6H_6, (e) $C_{20}H_{12}$, and (f) COD; IEEMD processed results for (g) C_6H_6, (h) $C_{20}H_{12}$, and (i) COD

Tab.3 Three parameters fitting functions and correlation coefficients

Parameter	Algorithm	Fitting function	R^2
C_6H_6	EMD	y=116.91x+187.94	0.862 7
	EEMD	y=31.171x+349.91	0.891 7
	IEEMD	y=27.725x+371.75	0.911 4
$C_{20}H_{12}$	EMD	y=71.292x-21.656	0.899 7
	EEMD	y=14.424x+143.29	0.926 9
	IEEMD	y=12.644x-1.986 4	0.980 1
COD	EMD	y=0.039 9x+0.497 9	0.974 7
	EEMD	y=0.038 4x+0.491 6	0.950 4
	IEEMD	y=0.036 2x+0.507 4	0.987 3

quality parameters (C_6H_6, $C_{20}H_{12}$, COD) are used as study objects in this work. The spectral signals of C_6H_6, $C_{20}H_{12}$, and COD are denoised based on the IEEMD and combined with multi-parameter detection technology of water quality, the *SNR* and the R^2 obtained after processing by the IEEMD are compared with the results obtained by the EMD and the EEMD. The experimental results show that the *SNR* of the 0.1 mg·L^{-1} C_6H_6 spectral signal is increased by 30.89% and 20.14%, respectively; the *SNR* of the 0.004 mg·L^{-1} $C_{20}H_{12}$ spectral signal is increased by 56.54% and 30.06%, respectively; the *SNR* of the 4 mg·L^{-1} COD spectrum signal increased by 8.82% and 11.79%, respectively; the R^2 of the C_6H_6 fitting curve is increased by 5.65% and 2.21%, respectively; the R^2 of the $C_{20}H_{12}$ fitting curve increased by 8.94% and 5.74%, respectively; the R^2 of the COD fitting curve increased by 1.29% and 3.88%, respectively. Therefore, the IEEMD effectively improves the accuracy and the stability of extracting multi-parameter spectral signals of water quality and provides an important experimental basis and research support for the efficient and rapid detection of water quality with multi-parameter in the future.

Ethics declarations

Conflicts of interest

The authors declare no conflict of interest.

References

[1] LI W, WANG L M, CHENG L, et al. Study on a multi-parameter method for the determination of water quality by sequential injection-continuous spectroscopy[J]. Spectroscopy and spectral analysis, 2021, 41(02): 612-617.

[2] HUANG X T, CHEN Y X, ZHU Z B, et al. Research progress on the detection of ascorbic acid based on nanomaterials spectroscopicanalysis[J]. Chinese journal of applied chemistry, 2021, 38(06): 637-650.

[3] XUE P, HE H, WANG H M. Error correction algorithm for optical measurement system based on radial basis function network[J]. Journal of optics, 2020, 40(02): 106-112. (in Chinese)

[4] LI Q B, WEI Y, CUI H X, et al. A quantitative method for water quality TOC analysis based on UV-Vis spectroscopy[J]. Spectroscopy and spectral analysis, 2022, 42(02): 376-380.

[5] YANG G F, DAI J C, LIU X J, et al. Spectral feature extraction based on continuous wavelet transform and image segmentation for peak detection[J]. Analytical methods, 2020, 12(2).

[6] VOUSOUGHI F D. Wavelet-based de-noising in groundwater quality and quantity prediction by an artificial neural network[J]. Water supply, 2023, 23(3).

[7] HUANG N E, SHEN Z, LONG S R. The empiricalmode decomposition and Hilbert spectrum for non-linear and non-stationary time series analysis[J]. Proceeding of the royal society of London, 1998, 454: 903-995.

[8] WU Z H, HUANG N E. Ensemble empirical mode decomposition: a noise-assisted data analysis method[J]. Advances in adaptive data analysis, 2009, 1(1): 1-41.

[9] ZOU N, JIN Y C, GUO C, et al. Preprocessing of radar signals in wells based on EMD[J]. Journal of the university of electronic science and technology, 2022, 51(06): 875-883. (in Chinese)

[10] LIANG Y, LIU T G, LIU K, et al. Optimization method of gas detection based on variational modal decomposition algorithm[J]. Chinese journal of lasers, 2021, 48(07): 135-144. (in Chinese)

[11] CAO L L, LI J, PENG Z, et al. Research on rolling bearing fault diagnosis based on EEMD and fast spectral cliffness[J]. Journal of mechanical & electrical engineering, 2021, 38(10): 1311-1316. (in Chinese)

[12] XU J, ZHANG B Y, FU Q. Study on differential noise reduction technique in infrasound calibration[J]. Academic journal of engineering and technology science, 2022, 5(13).

[13] ZHENG J D, CHENG J S, YANG Y. Improved EEMD algorithm and its application research[J]. Journal of vibration and shock, 2013, 32(21): 21-26+46. (in Chinese)

[14] CHEN J, KAN D, SUN T H, et al. Fault diagnosis method for rolling bearings based on SVD-VMD and SVM[J]. Journal of electronic measurement and instrumentation, 2022, 36(01): 220-226. (in Chinese)

[15] ZHANG R, ZHANG P, ZHAO F. Research on blast shock wave denoising algorithm based on CEEMDAN-SG[J]. Foreign electronic measurement technology, 2022, 41(10): 119-125. (in Chinese)

[16] LI M, ZHAO Y, CUI F P, et al. Characterization of Raman spectral signals based on ensemble empirical modal decomposition[J]. Spectroscopy and spectral analysis, 2020, 40(01): 54-58. (in Chinese)

[17] LI W, CAI Y Q, MA Y Y, et al. Design of a dual-spectrum water quality multi-parameter integrated system based on embedded technology[J]. Instrument technique and sensor, 2022, 469(02): 101-106.

[18] WANG X P, LIU Y F, TIAN T, et al. Research on the detection and simulation of water pollutants based on spectroscopic technology[J]. Journal of Huazhong University of Science and Technology (natural science edition), 2020, 48(03): 81-85+109.

[19] LI J, WANG W B, SHENG L, et al. A noise reduction method for microseismic signals applying bidirectional long and short term memory neural networks[J]. Oil geophysical prospecting, 2023, 58(02): 285-294.